2005

Nonlinear dynamics of piezoelectric high displacement actuators in cantilever mode

Timothy Usher
California State University - San Bernardino, tusher@csusb.edu

Alec Sim
Utah State University

Nonlinear dynamics of piezoelectric high displacement actuators in cantilever mode

Cite as: J. Appl. Phys. **98**, 064102 (2005); https://doi.org/10.1063/1.2041844
Submitted: 07 January 2005 . Accepted: 01 August 2005 . Published Online: 19 September 2005

Tim Usher, and Alec Sim

Nonlinear dynamics of piezoelectric high displacement actuators in cantilever mode

Tim Usher[a] and Alec Sim[b]
Department of Physics, California State University San Bernardino, 5500 University Parkway, San Bernardino, California 92407-2397

(Received 7 January 2005; accepted 1 August 2005; published online 19 September 2005)

Experimental results of the nonlinear dynamic response of a piezoelectric high displacement actuator known as thin-layer composite unimorph ferroelectric driver and sensor were compared to a theoretical model, which utilizes the multiple scales method to connect the effective spring constant to higher-order stiffness constants c_4 of the piezoelectric layer. This type of actuator has prestress gradients resulting from the manufacturing process that have been reported to play an important role in enhanced actuation. A value of $c_4=-4.7\times10^{20}$ N/m^2 was obtained for the higher-order lead zirconate titanate (PZT) stiffness coefficient, which is higher than other published results for PZT without prestress gradients. Peak resonance displacements over 1 mm were obtained for even small (100 V_{pp}) applied fields. The analysis showed a slight voltage dependence that was not specifically accounted for in the theory. This was confirmed by recasting data from other published results and further confirmed by dc offset studies reported here. © *2005 American Institute of Physics*. [DOI: 10.1063/1.2041844]

I. INTRODUCTION

Piezoelectric actuators play an increasingly important role in a variety of technological applications. For example, piezoelectric stack actuators are used in a variety of ways in scanning microscopes.[1] As the limits of scanning microscopes are pushed, the higher-order nonlinear material properties of the piezoelectric material play an increasingly important role. More recently, cantilevers with piezoelectric patches have been used as probes in some atomic force microscopes[1] (AFMs) where a clear understanding of the frequency response is essential. In many other applications,[2] it is desirable to operate the actuators at or near resonance where maximum displacements occur. However, these are precisely the conditions under which nonlinear effects are most pronounced. Historically, one disadvantage of traditional piezoelectric actuators is the fact that they produce small displacements compared to other actuator technologies. Efforts have been made to trade off the high pressure (forces) developed by piezoelectrics for greater displacements. Unfortunately, mechanical leveraging systems suffer numerous shortcomings. Early efforts to find alternatives to mechanical leveraging systems led to the development of Moonie actuators.[3] Later, Haertling[4] advanced the concept of a composite design, which has economic advantages in manufacturing. The actuator is known as reduced and internally biased oxide wafer (RAINBOW). More recently, a similar actuator was developed[5] in which a polyamide adhesive (LaRC™-SI), developed by NASA, was used to bond a metal substrate to a piezoelectric material at elevated temperatures inside an autoclave. In keeping with the meteorological theme, these actuators are known as thin-layer composite unimorph ferroelectric driver and sensor (THUNDER®). The components of a typical THUNDER actuator are illustrated in Fig. 1. Additional construction details are given in an article by Mossi *et al.*[6] The dimensions, thickness t, width b, length L, and density ρ pertaining to a particular type of actuator that was utilized in this investigation are given in Table I. The elastic compliance constant S_E^{11} at constant electric field E for the lead zirconate titanate (PZT) layer is 16.5×10^{-12} m^2/N. The subscripts denote the stress-strain directions where the 1 direction is along the poling direction. Young's modulus Y_s for the steel substrate is 2.0×10^{11} N/m^2. THUNDER® actuators are now commercially produced by Face International and some of their characteristics have been studied.[7] However, several questions remain unanswered for both RAINBOW and THUNDER® actuators. One important question is related to the effects of internal prestress gradients introduced during the manufacturing process that may impact the piezoelectric material properties. Li *et al.* make a strong argument, in the case of RAINBOW, that the effects make a significant contribution.[8] However, equivalent studies for THUNDER have not been conducted. Enhanced material properties in piezoelectrics have also been reported in the case of engineered domains.[9] Of particular relevance in this report is the possible impact of the internal prestress on the higher-order nonlinear material

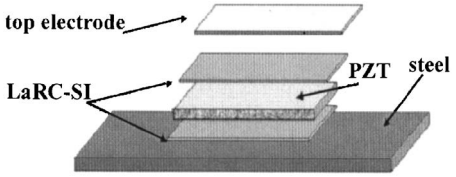

FIG. 1. Typical high displacement actuator construction. After bonding of adhesive at elevated temperature, the actuator obtains a characteristic curvature.

[a]Author to whom correspondences should be addressed; electronic mail: tusher@csusb.edu
[b]Present address: Department of Physics, Utah State University.

TABLE I. Properties of 11R THUNDER actuator.

Material	t (mm)	b (mm)	L (mm)	ρ (kg/m^3)
PZT	0.200	15.0	77.0	7.80×10^2
Stainless	0.152	15.0	77.0	7.87×10^2

properties. To address this question, we report experimental results of the frequency response of THUNDER actuators in cantilever mode for various excitation voltages. The results are compared to a theoretical development that connects the effective spring constant to the higher-order stiffness constants of the piezoelectric material.

II. THEORY

A theoretical treatment of the nonlinear response of a cantilevered beam can be found in the book by Nayfeh and Mook[10] as well as in other places. Wolf and Gottlieb adapted the theory to the case of a noncontacting atomic force microscope cantilever[11] and to a cantilever beam actuated by piezoelectric layers.[12] The following is, in large part, a summary of their theoretical development. Readers wishing to fully explore the details of the theoretical development are strongly encouraged to study Ref. 12. Slightly different notation is used. For a piezoelectric cantilever actuator, such as the one considered here, the nonlinear constitutive equations, modified for the particular geometry can be expressed as follows:

$$T_1 = -e_{31}^L E_3 + c_2 S_1 + \tfrac{1}{2}c_3 S_1^2 + \tfrac{1}{6}c_4 S_1^2,$$
$$D_3 = \varepsilon_{33}^L E_3 + e_{31}^L S_1, \tag{1}$$

where T_1 and S_1 are the longitudinal (along the long direction) stress and strain, respectively. In addition, D_3 and E_3 are the electric displacement and electric field in the transverse direction (along the thin direction). The coefficients c_3 and c_4 are the nonlinear stiffness coefficients of particular interest in this investigation.

The linear material constants for the piezoelectric are as follows:

$$c_2 = 1/s_{11}^E,$$
$$e_{31}^L = \frac{d_{31}}{s_{11}^E}, \tag{2}$$
$$\varepsilon_{33}^L = \varepsilon_{33}^T(1-k_{31}^2).$$

Here c_2 is the linear elastic stiffness coefficient and S_{11}^E was defined earlier. The constant k_{31} is the electromechanical coupling factor, d_{31} is the piezoelectric constant perpendicular to the direction of the electric field, e_{31}^L is the piezoelectric stress constant, and ε_{33}^L is the permittivity. The superscripts indicate constant (zero) stress (T), constant (short circuit) electric field (E), and constant strain (L).

According to the Bernoulli-Euler hypothesis, it is assumed that the layer of thickness dz remains plane and perpendicular to the neutral axis of the cantilever. The neutral axis η is given by the following expression:

$$\eta = \frac{1}{2}\frac{(t_s^2 Y_s - t_p^2 c_2)}{(t_s Y_s + t_p c_2)}, \tag{3}$$

where t_p is the thickness of the piezoelectric, t_s is the thickness of the substrate, and Y_s is the Young's modulus of the substrate. The equations of motion for the beam are derived from Hamilton's principle. The material properties of the piezoelectric layers are represented by the electric enthalpy density. The enthalpy can be expressed in terms of a fourth-order polynomial that provides a connection between the piezoelectric material and its response to the applied electric field. The constants c_3 and c_4 are nonlinear material constants. The electric enthalpy per unit length can be expressed in terms of a polynomial with the following coefficients:

$$H_{20} = -\frac{b}{t_p}\varepsilon_{33}^L,$$
$$H_{11} = -\tfrac{1}{2}b(2\eta + t_p)e_{31}^L,$$
$$H_{02} = \frac{1}{12}b\left[t_p^3\frac{e_{31}^{L^2}}{\varepsilon_{33}^L} + 4(t_p^3 + 3t_p^2\eta + 3t_p\eta^2)c_2 + 4(t_s^3 - 3t_s^2\eta + 3t_s\eta^2)Y_s\right], \tag{4}$$
$$H_{03} = \tfrac{1}{8}b(t_p^4 + 4t_p^3\eta + 6t_p^2\eta^2 + 4t_p\eta^3)c_3,$$
$$H_{04} = \tfrac{1}{30}b(t_p^5 + 5t_p^4\eta + 10t_p^3\eta^3 + 5t_p\eta^4)c_4,$$

where b is the width of the cantilever. The Lagrangian can be written in terms of the electric enthalpy per unit length. Taking the variation of the Lagrange density and expanding the angular displacement of the beam to third order in the linear displacement lead to the equations of motion for the system. (See Ref. 12 for details.)

The following dimensionless spatial ξ and temporal τ quantities are useful for the remainder of the theoretical development:

$$\xi \equiv \frac{x}{L} \tag{5}$$

and

$$\tau \equiv t\sqrt{\frac{H_{02}}{\rho_A L^4}}, \tag{6}$$

where the dimensional spatial x and temporal t quantities have appropriate units. The length of the actuator is given by L and ρ_A is the average linear density (mass/length) of the actuator. H_{02} is given by Eq. (4). Incidentally, Eq. (6) corrects a typographical error in Wolf and Gottlieb's paper.[12]

In accordance with the multiple scale method, the response of the cantilever can be represented via three different time scales, which are distinguished in their order of magni-

tude by a small dimensionless parameter δ. The linear displacement can also be expanded in terms of the parameter δ. This method eventually leads to the eigenmode solutions for the clamped beam,

$$\Phi_n(\xi) = \cosh(z_n\xi) - \cos(z_n\xi) - A_n[\sinh(z_n\xi) - \sin(z_n\xi)] \tag{7}$$

with $z_n = \omega_n{}^{1/2}$, where ω_n is the nth (angular) eigenmode frequency and

$$A_n = \frac{\cosh(z_n) + \cos(z_n)}{\sinh(z_n) + \sin(z_n)} \tag{8}$$

is determined numerically from the nth root of the characteristic equation

$$1 + \cosh(z_n)\cos(z_n) = 0. \tag{9}$$

We can assume a driving voltage at a frequency Ω and amplitude $U_{\max}$. Furthermore, we can introduce a dimensionless damping coefficient μ. It is also customary to introduce a detuning parameter σ where

$$\Omega = \omega_1 + \delta^2\sigma \tag{10}$$

and the corresponding normalized damping coefficient $\bar{\mu} = \delta^2\mu$. The bar indicates that it is normalized.

With these definitions and further analysis, we ultimately arrive at the evolution equation, which can be solved to yield the following important result for the response amplitude a_1 for the primary (as denoted by the subscripts 1) resonance peak:

$$\sigma = \frac{\gamma_c}{\omega_1}a_1^2 \pm \frac{1}{2}\sqrt{\left(\frac{\gamma_{12}\alpha_{12}U_{\max}}{a_1\omega_1}\right)^2 - \mu^2}. \tag{11}$$

The + in Eq. (11) corresponds to frequencies below the resonance peak. The − in Eq. (11) corresponds to frequencies above the resonance peak. The effective spring constant γ_c is given by the following expression:

$$\gamma_c = \left(\tfrac{3}{8}\alpha_1 + \tfrac{9}{8}\gamma_{42}\alpha_{42} - \tfrac{1}{4}\gamma_{32}{}^2\alpha_{32} - \tfrac{1}{2}\alpha_2\omega_1^2\right) \tag{12}$$

with

$$\alpha_1 = \int_0^1 \Phi_1[\Phi_1'(\Phi_1'\Phi_1'')']'d\xi, \tag{13}$$

$$\alpha_{42} = \int_0^1 \Phi_1[(\Phi_1'')^3]''d\xi \tag{14}$$

$$\alpha_2 = \int_0^1 \Phi_1\frac{1}{2}\left[\Phi_1'\int_1^\xi\int_0^s(\Phi_1')^2 d\xi ds\right]'d\xi, \tag{15}$$

$$\alpha_{12} = \Phi_1'(1). \tag{16}$$

The primes indicate spatial derivatives. The gammas are given by the following expressions.

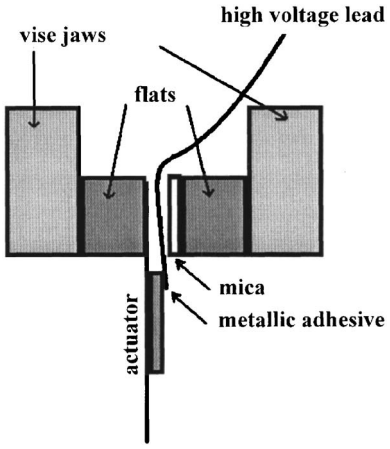

FIG. 2. Mechanical test fixture for clamping the actuator. Proper clamping is essential for reproducible results.

$$\gamma_{12} = L\frac{H_{11}}{H_{02}},$$

$$\gamma_{32} = \frac{1}{L}\frac{H_{03}}{H_{02}}, \tag{17}$$

$$\gamma_{42} = \frac{1}{L^2}\frac{H_{04}}{H_{02}}.$$

It is convenient to normalize the higher-order coefficients with respect to the linear coefficient c_2 according to

$$K_{32} = \frac{c_3}{c_2} \quad \text{and} \quad K_{42} = \frac{c_4}{c_2}. \tag{18}$$

In the case of the experimental work considered here, $\gamma_{32} = 6.76\times10^{-4}K_{32}$ and $\gamma_{42} = 4.96\times10^{-7}K_{42}$. The numerical factors are particular to the cantilevers used in this investigation. Equation (12) relates the spring constant to γ_{42} and γ_{32}, which are in turn related to the higher-order stiffness coefficients K_{42} and K_{32}. Notice that the K_{42} and K_{32} terms enter with opposite signs. Further, note that γ_{32} is squared, whereas γ_{42} is not, making the γ_{32} term insensitive to the sign of K_{32} while the γ_{32} term is sensitive to the sign of K_{42}. Arguments will be given later for dropping the third term involving α_{32}.

The reader is reminded that the derivation is in terms of dimensionless quantities, which need to be accounted for when comparing to experimental results.

III. EXPERIMENTAL PROCEDURES

The experimental setup can be conceptually divided into mechanical and electrical components. Figure 2 depicts the mechanical arrangement and Fig. 3 depicts the electrical connections. The data acquisition and control process were computer automated. The stimulation signal was initially generated by an arbitrary function generator, amplified and then applied to the actuator. The actuator response was measured by a laser micrometer. The applied voltage and laser response were acquired via two channels of a data acquisition card.

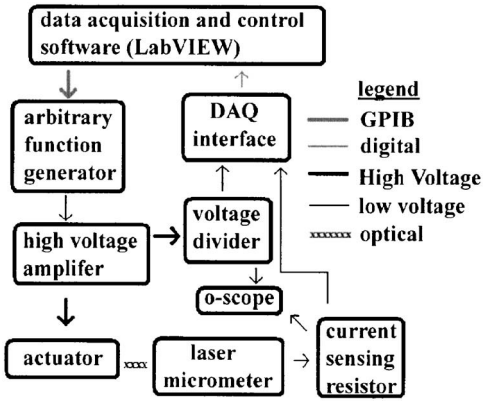

FIG. 3. Electrical signal and data acquisition arrangements.

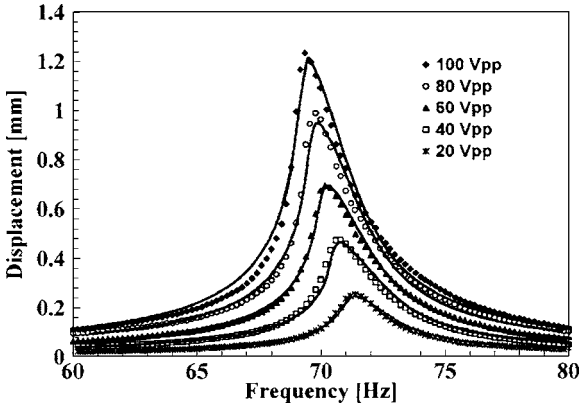

FIG. 4. Typical family of frequency response curves taken at different applied voltage amplitudes for an 11R actuator. The vertical scale is in terms of peak displacement. The curves are fits to Eq. (11).

A. Mechanical

Actuators were mounted mechanically in a cantilever configuration with displacement in the horizontal plane to avoid acceleration errors at high displacement and/or frequency values. Whenever possible, standard, easily accessible components were used rather than specially fabricated components in order to promote repeatability by other researchers. Two steel machine flats were clamped inside the jaws of a Craftsman® 24073 drill press vise, which was mounted on a Newport® EG 32-2 optical bench. It was not necessary to utilize the vibration isolation capabilities of the optical bench. The actuator was clamped between the machine flats in order to provide a hard cantilever clamp. A variety of measured torques for the vise were employed to verify that the torque did not affect the results. It was critical to avoid mechanical parasitic effects due to the electrical leads. This was accomplished by feeding the electrical contacts through the mechanical clamps. The details of the electrical leads are described below.

B. Electrical

The original actuator electrical leads supplied by the factory were removed and thin flexible copper traces were used as leads. The traces were approximately 2 mm wide and 0.2 mm thick. They were bonded to the top aluminum electrode using Master Bond® EP211TDCHT metallic adhesive. The thin outline and increased width of the copper leads allowed for good contact and stable nonparasitic connection for the duration of the study. However, this configuration could be improved as it is both difficult to implement and will suffer stress degradation over very long periods of use. The thin electrical leads were fed through the clamp. A thin sheet of mica served as extra high-voltage insulation. The bottom steel substrate served as the other electrode and was connected to ground via the metal clamp.

National Instruments® software, LABVIEW® 6.1, running on a Dell® computer with a Pentium® processor and Microsoft® Windows® operating system was used to automate the data acquisition and control. An arbitrary function generator (HP 33120A), under computer control via a GPIB (IEEE 488.2) interface, was used to produce a low-voltage signal, which was then amplified with a high-voltage amplifier (Kepco® BOP-1000M) and then applied to the actuator. The applied voltage was monitored by one of the channels of a National Instruments® data acquisition card (NI DAQ 6024E) after a passive voltage divider. A laser charge-coupled device (CCD) micrometer (Micro-Epsilon® IDL-1400) was used to measure the displacement. The current output of the micrometer was passed through a resistor providing a conversion from current to voltage. The voltage across the resistor was then monitored by another channel of the data acquisition card. We calibrated the laser micrometer against a Michelson-Morley interferometer over the entire range of the micrometer (5 mm). This was accomplished by automating the fringe counting process, thereby providing an extremely accurate distance measurement. The calibration curve was very linear, so a simple multiplicative factor was used to convert micrometer voltage to a displacement. An oscilloscope (HP5403B) was used to independently monitor the applied high voltage and micrometer output voltage. In addition to serving as an independent verification of the acquired data, this configuration was used to monitor the phase relation between the applied high voltage and the micrometer displacement voltage. In this way any signal coupling, degradation, or anomalous behavior between the supply and the actuator could be observed *in situ*.

Data collection and reduction was integrated into the LABVIEW® code and allowed for frequency and voltage stepping. The reduced data profiles then consist of a spectrum of voltages and frequencies/tones centered about the expected resonant frequency (see Fig. 4). A single tone data set (raw data) consists of 512 points sampled at 990 S/s (samples per second), where the update rate of the IDL-1400 is 1024 S/s. Since the sampled frequencies were much less than the DAQ or IDL-1400 sampling rate, we reduced the DAQ rate to avoid over-sampling. Typical frequency spans are +/−20 Hz, about the center tone, to allow for asymptotic behavior to appear. The first resonant modes for actuators considered here were below 120 Hz. In addition, a wait time was associated with each frequency, prior to collection, to avoid initial transient effects. Both the wait time and the center frequency were determined empirically prior to operation. These parameters and sampling rates provided ample data density for the reduction process. The micrometer response voltage and dc offset for a given tone were first cal-

culated, and then the single tone frequency was obtained using standard fast Fourier transform (FFT) techniques. This provided a single data point (V, Hz) in the dynamic response curve. Then, for a single applied voltage, we obtain a range of frequency and micrometer response voltage points that compose a single response curve in the voltage domain (see Fig. 4). The data were then converted from volts to meters using the previously mentioned conversion factors. In addition, for each response curve the peak and center frequencies were calculated using a standard singular value decomposition peak fitting routine. From this and the original data, frequency versus voltage and peak displacement versus voltage plots were obtained. The error in the data sets follows largely from the calibrations as the fitting algorithms yield very small error contributions. The details of the calibrations and complete error analysis are omitted. However, we considered a spectrum of error sources including temperature, power, and drift of the electronics in addition to parasitic energy losses, inductive/capacitive coupling, and the full spectrum response of all instruments beyond the required ranges. Furthermore, the amplifier was carefully monitored to ensure that it did not deviate from the expected voltage as a result of the highly reactive load near resonance. The final worst-case errors for frequency, applied voltage, and displacement, respectively, are as follows: +/−0.1 Hz, +/−0.1 V, and +/−0.1 mm.

IV. RESULTS

We focused on the Face International 11R THUNDER® actuator. The other models showed similar results. However, they were not as extensively investigated. Six 11R actuators were investigated with similar results for each actuator. A typical set of experimental (data points) nonlinear response curves are shown in Fig. 4 along with the fit to theory (smooth curve).

The resonance curves shown in Fig. 4 clearly show a nonlinear response. The response amplitude was kept small to avoid the jump phenomena typical of nonlinear systems. The peaks shifted towards lower frequencies with increasing drive voltage amplitudes, indicating a softening of the effective spring constant. The results compare favorably with the theory by Wolf and Gottlieb.[12]

By inspecting Eq. (11), it can be seen that for a given drive voltage, the peak amplitude a_{1p} occurs when the two terms inside the square root are equal,

$$\mu_1^2 = \left(\frac{\gamma_{12}\alpha_{12}U_{\max}}{a_{1p}\omega_1} \right)^2. \tag{19}$$

This expression can be rearranged to give a linear relation between the peak response amplitude a_{1p} and the maximum applied voltage $U_{\max}$,

$$a_{1p} = \frac{\gamma_{12}\alpha_{12}}{\mu_1\omega_1}U_{\max}. \tag{20}$$

Figure 5 represents typical experimental results showing a linear relation in good agreement with theory.

In order to further compare quantitatively the experimental results with theory, it is necessary to obtain an independent value for the dimensionless damping coefficient μ. This was done experimentally by manually displacing the cantilever tip and suddenly releasing it, resulting in a free decay vibration, which was monitored electronically via the direct piezoelectric effect and monitored mechanically via the laser micrometer. A typical decay response is shown in Fig. 6. Inspection of the shape of the curve confirms the assumption of linear damping as opposed to quadratic, Coulomb, or hysteretic damping. (See Sec. 3.3.3 in Ref. 10.) The damping curves yield an independent value for the damping coefficient of 6.90 1/s and using Eq. (6), a dimensionless value of μ=0.119. This, in turn, yields a value for the small order parameter δ=0.0279 that is used in further calculations discussed later.

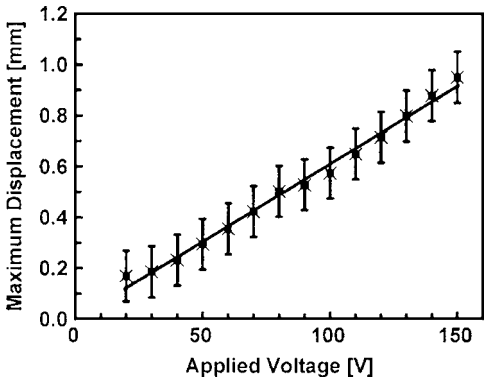

FIG. 5. Typical maximum amplitude response as a function of applied voltage (peak to peak) for an 11R actuator. Data is for an 11R actuator other than actuators presented in other figures.

Now turning our attention to the first term in Eq. (11) which is left after setting the last term equal to zero, we have the following linear relation between the detuning parameter and the square of the peak amplitude,

$$\sigma = \frac{\gamma_c}{\omega_1}a_{1P}^2. \tag{21}$$

The curve prescribed by this equation is commonly referred to as the backbone curve. Figure 7 shows some typical ex-

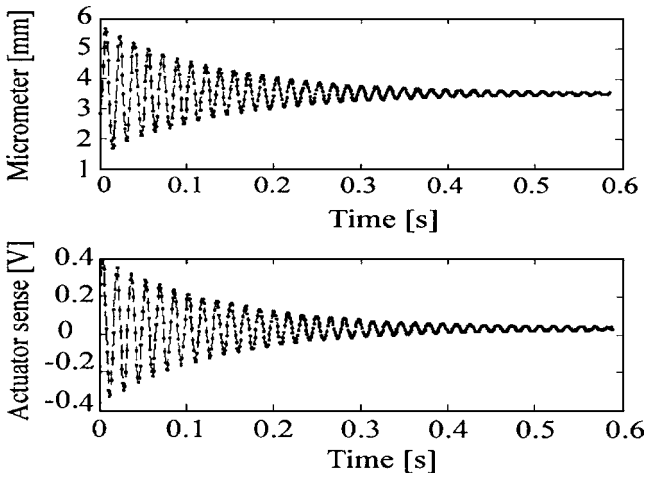

FIG. 6. Typical free decay of 11R actuator. The decay is monitored by the laser micrometer and by the actuator in sensor mode. The micrometer decay includes an unimportant offset.

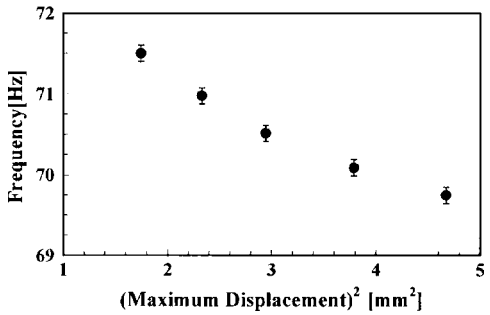

FIG. 7. Peak resonance frequency plotted against maximum amplitude squared for a typical 11R actuator response. The horizontal error bars are smaller than the data point symbol.

perimental results. A straight line could be drawn through the data points and still remain within experimental error. However, there is a clear indication of curvature, which will be discussed later. Assuming a linear fit, the experimental data gives a value of -2.6×10^5 Hz/m^2 for the slope. This slope can then be used to calculate a value for the effective spring constant γ_c. The effective spring constant is negative (softening). It is important to keep in mind that the relations given in Eq. (5) and (6) must be used to compare experimental and theoretical values.

The effective spring constant is given by Eq. (12). Other experiments[13] have shown that that the relative stiffness coefficient K_{32} is small so the third term will be dropped resulting in the following expression:

$$\gamma_c = \left(\tfrac{3}{8}\alpha_1 + \tfrac{9}{8}\gamma_{42}\alpha_{42} - \tfrac{1}{2}\alpha_2\omega_1^2\right). \tag{22}$$

Assuming a straight line for Fig. 7, the slope leads to a value of $c_4=-4.8\times10^{20}$ N/m^2 for the higher-order stiffness coefficient. Other experimental values for c_4 are scarce in the literature. Furthermore, they vary widely from -2.4×10^{16} to -1.4×10^{18} N/m^2 depending on the particular PZT formulation used. One publication by von Wagner and Hagedorn[14] reports $c_4=-1.4\times10^{18}$ N/m^2. However, different PZT formulations were used. Morgan Electroceramics PZT-5A ceramics were used in our work and von Wagner and Hagedorn used PIC 151 manufactured by PI-Ceramic. The higher c_4 value in the case of high displacement THUNDER actuators may be associated with the prestress. However, further studies need to be conducted to be certain. Our value for c_4 is larger than those reported by others. Referring to Eq. (1), it is interesting to examine the relative contributions of the term involving the higher-order stiffness coefficient c_4 with the linear term involving the linear coefficient c_2. Even for strains as small as 250 μm/m (typical strains for PZT can be as high as 1200 μm/m), the contribution of the nonlinear term is of the same order of magnitude as the linear term. Unfortunately, the need to avoid experimental complications associated with the jump phenomena at high amplitudes results in decreased dynamic range and consequently decreased sensitivity to the value of the effective spring constant. In future experiments it may be possible to improve sensitivity by exploring higher-order resonance modes. However, these results indicate that the effective spring constant depends on voltage. This dependence should be more pronounced at higher amplitudes (higher drive voltages). The curvature in Fig. 7 could be explained by a voltage-dependent spring constant γ_c, which is not specifically accounted for in the theory.

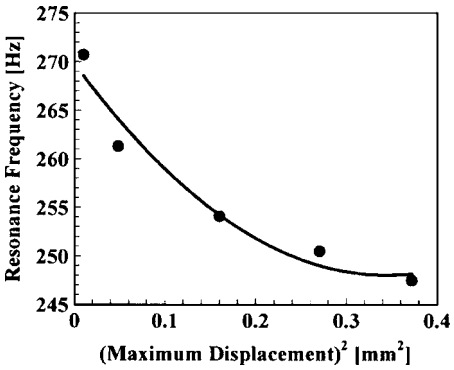

FIG. 8. Peak resonance frequency plotted against maximum amplitude based on results from Wang *et al.* (see Ref. 15). The smooth curve is a guide for the eye.

Comparable results were reported by Wang *et al.*[15] from Cross's laboratory for RAINBOW actuators and by Ounaies *et al.*[16] for THUNDER actuators. Wang *et al.* investigated nonlinear behavior in RAINBOW actuators, which were the predecessors of THUNDER actuators. Although their theoretical treatment is quite different from the one presented here, the experimental results are similar. Figure 8 shows an adaptation of their experimental data to the analysis used here. Their data shows the same voltage-dependent behavior as seen in our data Fig. 7.

In an attempt to separate, to the extent possible, mechanical response characteristics from electrical response characteristics we applied a small ac voltage with a large dc voltage. The results are shown in Fig. 9. These results show a clear dc voltage dependence. The very strong dependence at large negative dc voltages may be due to the onset of depoling.

V. CONCLUSIONS

The coupling of electric and mechanical fields is the defining characteristic of piezoelectric materials. First-order coefficients have been thoroughly investigated even though relatively recent surprises[17] have been discovered in $BaTiO_3$, which is one of the most widely studied piezoelectric materials. Higher-order coefficients are not as widely known.

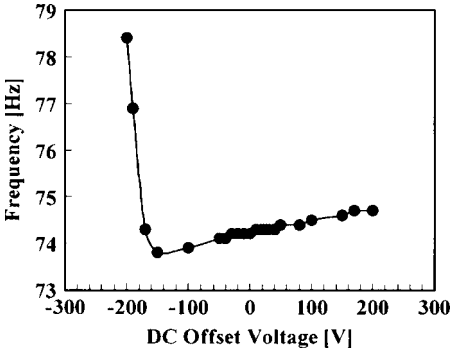

FIG. 9. Typical resonance response as a function of dc offset voltage for an 11R actuator. The smooth curve is a guide for the eye.

However, they are important in applied studies as well as those that are more fundamental. This report connects a nonlinear theory with experimental results on prestress-gradient piezoelectric actuators. Our results compare favorably with the theory, as well as other experimental results, providing insight into piezoelectric material properties. The results indicate that the prestress gradients have minimal impact on the higher-order stiffness coefficients. However, the effective spring constant exhibits a voltage dependence that is not accounted for. This conclusion is confirmed by reconstituted data from other published results as well as our dc offset results. This may warrant further study.

ACKNOWLEDGMENTS

The authors thank Adalia Cabanyog, Gilberto Camargo, Gevale Ashford, and Monica Marcial-Armenta for their contributions. Ken Ulibarri has earned special recognition for his early contributions to the research. The technical assistance of Jan Mack and James Sheu is also gratefully acknowledged. This research was funded by a NASA Faculty Awards for Research Grant No. 0051-0078.

[1]F. J. Giessibl, Rev. Mod. Phys. **75**, 949 (2003).
[2]J. A. Palmer, B. Dessent, J. F. Mulling, T. Usher, E. Grant, J. W. Eischen, A. I. Kingon, and P. D. Franzon, IEEE/ASME Trans. Mechatron. **9**, 392 (2004).
[3]Y. Sugawara, K. Onitsuka, S. Yoshikawa, Q. C. Xu, R. E. Newnham, and K. Uchino, J. Am. Ceram. Soc. **75**, 996 (1992).
[4]G. H. Haertling, Am. Ceram. Soc. Bull. **73**, 93 (1994).
[5]R. F. Hellbaum, R. G. Bryant, and R. I. Fox, U.S. Patent No. 5632841 (27 May 1997).
[6]K. M. Mossi, G. V. Selby and R. G. Bryant, Mater. Lett. **35**, 39 (1998).
[7]J. Mulling, T. Usher, B. Dessent, J. Palmer, P. Franzon, E. Grant, and A. Kingon, Sens. Actuators, A **94**, 19 (2001).
[8]G. Li, E. Furman, and G. H. Haertling, J. Am. Ceram. Soc. **80**, 1382 (1997).
[9]R. C. Rogan, N. Tamura, G. A. Swift, and E. Ustundag, Nat. Mater. **2**, 379 (2003).
[10]A. H. Nayfeh and D. T. Mook, *Nonlinear Oscillations* (Wiley, New York, 1997).
[11]K. Wolf and O. Gottlieb, J. Appl. Phys. **91**, 4701 (2002).
[12]K. Wolf and O. Gottlieb, Technion-Israel Institute of Technology Report No. ETR-2001-02, 2001.
[13]W. Jiang and W. Cao, J. Appl. Phys. **88**, 6684 (2000).
[14]U. von Wagner and P. Hagedorn, J. Sound Vib. **256**, 861 (2002).
[15]Q. M. Wang, Q. Shang, B. Xu, R. Liu, and L. E. Cross, J. Appl. Phys. **86**, 3352 (1999).
[16]Z. Ounaies, K. Mossi, R. Smith, and J. Bernd, NASA/CR-2001-210859, ICASE Report No. 2001-9, 2001.
[17]S. Park, S. Wada, L. E. Cross, and T. R. Shrout, J. Appl. Phys. **86**, 2746 (1999).